Pharmaceutical Research, Vol. 24, No. 12, December 2007 (© 2007)
DOI: 10.1007/s11095-007-9454-6

Research Paper

Development of a Cell Transducible RhoA Inhibitor TAT-C3 Transferase and its Encapsulation in Biocompatible Microspheres to Promote Survival and Enhance Regeneration of Severed Neurons

Elaine Y. M. Tan,[1] Janice W. S. Law,[1,2] Chi-Hwa Wang,[3] and Alan Y. W. Lee[1,2,4]

Received July 1, 2007; accepted September 5, 2007; published online September 25, 2007

Purpose. Neurons in post-traumatized mammalian central nervous system show only limited degree of regeneration, which can be attributed to the presence of neurite outgrowth inhibitors in damaged myelin and glial scar, and to the apoptosis of severed central neurons and glial cells during secondary Wallerian degeneration. RhoA GTPase has been implicated as the common denominator in these counter-regeneration events, which shows significant and persistent up-regulation for weeks in injured spinal cord and cerebral infarct after stroke. While the exoenzyme C3 transferase is a potent RhoA inhibitor, its extremely low efficiency of cell entry and degradation *in vivo* has restricted the therapeutic value. This study aims to circumvent these problems by developing a membrane-permeating form of C3 transferase and a biopolymer-based microsphere depot system for sustainable controlled release of the protein.
Materials and Methods. A membrane-permeating form of C3 transferase was developed by fusing a Tat (trans-activating transcription factor) transduction domain of human immunodeficiency virus to its amino terminal using standard molecular cloning techniques. After confirming efficient cell entry into epithelial and neuroblastoma cells, the resulting recombinant protein TAT-C3 was encapsulated in biocompatible polymer poly(D,L-lactide-co-glycolide) in the form of microspheres by a water-in-oil-in-water (W/O/W) emulsion method. By blending capped and uncapped form of the polymer at different ratios, TAT-C3 protein release profile was modified to suit the expression pattern of endogenous RhoA during CNS injuries. Bioactivity of TAT-C3 released from microspheres was assessed by RhoA ribosylation assay.
Results. In contrast to wild-type C3 transferase, the modified TAT-C3 protein was found to efficiently enter NIH3T3 and N1E-115 neuroblastoma cells as early as 6 hours of incubation. The fusion of TAT sequence to C3 transferase imposed no appreciable effects on its biological activity in promoting neurite outgrowth through RhoA inhibition. Characterization of TAT-C3 encapsulation in various blends of capped/uncapped PLGA polymer revealed the 30:70 formulation to be optimal in attaining a mild initial burst release of 25%, followed by a subsequent average daily release of 2.3% of encapsulated protein over one month, matching the change in RhoA level in severed brain and spinal cord. Importantly, TAT-C3 released from the microspheres remained active up to the first three weeks of incubation.
Conclusion. Enhanced cell entry of TAT-C3 circumvents the need to administer high dose of the protein to site of injury. The encapsulation of TAT-C3 in different blends of capped/uncapped PLGA microspheres allows adjustment of protein release profile to suit the pattern of RhoA expression in injured CNS.

KEY WORDS: C3 transferase; controlled drug release; microspheres; poly(lactic-co-glycolic acid); RhoGTPases.

INTRODUCTION

In contrast to the peripheral nervous system, severed mammalian central neurons show very limited degree of regenerative capacity due to various unfavorable factors such as cell death and upregulation of regeneration inhibitors. Functional recovery after spinal cord injury (SCI) therefore remains to be a major challenge for neuroscientists. The cellular event immediately following injury of the spinal cord is typical post-traumatic necrosis of severed neurons and non-neuronal cells. It is often accompanied by subsequent Wallerian degeneration that involves apoptotic cell death in the lesion epicenter and in the adjacent white matter (1). Cells that undergo apoptosis include oligodendrocytes, microglia, and neurons (1,2). Activation of p75 neurotrophic receptor ($p75^{NTR}$) and RhoA have been implicated in apoptotic cell death of oligodendrocytes during Wallerian degeneration and lead to demyelination (3). Secondary

[1] Department of Physiology, Yong Loo Lin School of Medicine, National University of Singapore, Block MD9, 2 Medical Drive, Singapore 117597, Singapore.
[2] Neurobiology Program, Centre for Life Sciences, National University of Singapore, 28 Medical Drive, Singapore 117456, Singapore.
[3] Department of Chemical and Biomolecular Engineering, Faculty of Engineering, National University of Singapore, 4 Engineering Drive, Singapore 117576, Singapore.
[4] To whom correspondence should be addressed. (e-mail: phsleeyw@nus.edu.sg)

cellular degeneration gradually progresses and leads to chronic demyelination of oligodendrocytes in fiber tracts away from the site of injury. Oligodendrocyte degeneration causes the shedding of myelin debris, which can be cleared by activated microglia. Nonetheless, this process is not as efficient as their Schwann cell counterpart in the peripheral nervous system. This results in the persistence of myelin debris in injured spinal cord, which has been known to contain factors inhibitory to axon regeneration (4–6). To date, Nogo, myelin associated glycoprotein (MAG), and oligodendrocyte myelin glycoprotein (OMgp) have been identified as the three major myelin inhibitors that impede regeneration of neurons in mammalian central nervous system (CNS) (7). Recent findings suggest that these molecules share the same receptor complex between p75 neurotrophic receptor ($p75^{NTR}$) and Nogo receptor (NgR), which in turn signals through RhoA activation and induces growth cone collapse (8).

Lesion in the spinal cord is known to activate proliferation of astrocytes, which undergo hypertrophy and increase complexity of their processes. Intermingle of astrocytic processes with oligodendrocytes, meningeal cells, microglia, and fibroblasts gradually develop into a scar-like structure. Glial scar impedes axonal regeneration not only by imposing a physical barrier (4,9,10) but the presence of axonal growth inhibitory molecules in the scar seems to play a pivotal role (9). The chondroitin sulfate proteoglycans (CSPGs) family of molecules, like neurocan, versican, brevican, NG2, phosphacan, whose expression is upregulated following CNS injury (11–13), represent a major population of these inhibitory molecules that contribute to the failure of axon regeneration (13–15). Other inhibitory molecules found in glial scar include tenascins (16), semaphorin 3A (17,18), and semaphorin 4D (19). Interestingly, accumulating evidence suggests the inhibitory effects of both CSPGs and semaphorins are mediated through RhoA pathway (20–22).

Taken together, RhoA pathway represents a common denominator for the signaling of both apoptotic cell death during Wallerian degeneration and neurite outgrowth inhibition by major myelin inhibitors in injured spinal cord. Inhibition of RhoA activity and its downstream pathways therefore represents a potential point of therapeutic intervention to alleviate these counter-regeneration events. The exoenzyme C3 transferase from *Clostridium botulinum* has long been known to specifically inhibit RhoA by ADP-ribosylation of its effector domain (23). Accumulating evidence suggests beneficial effect of targeted inhibition of RhoA by C3 transferase or its effector Rho kinase (p160ROCK) by chemical inhibitor Y-27632 in promoting CNS neuronal regeneration (24–28). Nonetheless, the efficiency of this 24 kDa C3 protein to enter cell is very low because it lacks the cell surface binding and transport component typically found in other families of bacterial toxins. Aids to facilitate C3 cell entry include the use of high protein dosage or by physical means of protein delivery such as microinjection, trituration, or scrape-loading. While the former method suffers from potential cytotoxic effects, the mechanical stress and disruption of cell intactness associated with the latter techniques preclude their clinical applications in treating injured spinal cord. We describe in this study the development of a membrane-permeating form of C3 transferase by fusing a Tat (trans-activating transcription factor) transduction domain of human immunodeficiency virus (29,30) to its amino terminal. Tat domain is known to cross cell membrane even when fused with large heterologous protein (31). Major challenge in applying this TAT-C3 fusion protein in SCI treatment is the maintenance of its availability to the site of injury in bioactive form over the period during which intervention of RhoA pathway is the most effective. Previous findings in fact demonstrated significant up-regulation of RhoA for weeks in injured spinal cord and cerebral infarct after stroke (32,33). While repeated introduction of therapeutic proteins can partially address the issue of degradation and maintenance of supply, it may not be feasible in less accessible organs such as the brain and the spinal cord. To attain the goal of developing a sustainable *in vivo* release system for TAT-C3, we encapsulated the protein in a biocompatible and biodegradable polymer poly(D,L-lactide-co-glycolide) (PLGA) (34–36). The approach of blending capped and uncapped PLGA at different ratios allows rational design of microspheres that show low initial burst and constant release of TAT-C3 that sustains over extended period, implicating the potential use of this protein drug delivery system in SCI and stroke treatment.

MATERIALS AND METHODS

Materials

PLGA (lactide to glycolide ratio of 50:50) carrying uncapped (free carboxyl) and capped (lauryl ester) end groups with average molecular weight of 24,000 Da were purchased from MediSorb (Alkermes, Cincinnati, OH, USA). Polyethylene glycol (PEG, MW 3,350) was purchased from Sigma (St Louis, USA). Anti-HA and anti-RhoA antibodies were purchased from Santa Cruz Biotechnology (California, USA). C3 transferase cDNA was obtained from Dr. Lamarche V.N. at McGill University, Canada.

Cloning and Purification of TAT-C3 Transferase

The glutathione sulfotransferase (GST) expression vector pGEXKG-TAT carrying Tat sequence (YGRKKRRQ RRR) was built by inserting an annealed oligonucleotide pair (5'-GCATATGTACGGTCGTAAAAAACG TCGTCAGCGTCGTCGTGGT-3' and 5'-TAGACCAC GACGACGCTGACGACGTTTTTTACGACCGTACA TATGC-3') into pGEXKG vector (37) via SmaI and XbaI sites. It was then subcloned with C3 transferase cDNA carrying a hemagglutinin (HA) epitope tag (YPYDVPDYA) at XbaI and SacI sites to yield pGEXKG-TAT-C3. A similar plasmid lacking the Tat sequence but with HA tag was also constructed to serve as a control. To express C3 transferase as GST fusion protein, BL21 strain of *E. coli* bacteria harboring the expression construct were grown in Lauria broth (LB) medium overnight at 37°C. The culture was diluted in a 1:10 ratio in fresh LB broth and grown for an additional one hour. Expression of the GST fusion protein was induced by 0.5 mM isopropyl β-D-thiogalactoside (IPTG) for 3 hours at 37°C. The cells were pelleted by centrifugation, resuspended in 1× phosphate-buffered saline (PBS), and lysed by sonication (3 rounds of 15 sec burst with

15 sec interval). After pelleting insoluble cell debris, soluble fusion proteins were purified by affinity chromatography using glutathione sepharose 4B (Amersham Biosciences, Uppsala, Sweden) according to manufacturer's instructions. TAT-C3 protein was then released from the GST moiety by thrombin-mediated cleavage (10 units/ml for 9 hours at 4°C) and purified with p-aminobenzamidine agarose (Sigma, St Louis, USA) treatment. The protein was stored at −20°C until use.

Determination of Cell Permeability of TAT-C3 Transferase and its Neurite-outgrowth Promoting Effect on Neuroblastoma

The ability of purified TAT-C3 in gaining access into cells was determined by immunofluorescence detection upon incubation with NIH3T3 fibroblasts. Briefly, NIH3T3 cells were plated at a density of 2.7×10^4 cells on 12 mm circular glass coverslips in a 24-well culture dish and cultured in Dulbecco's modified Eagle's medium (DMEM) with 10% fetal bovine serum (FBS) and 1% penicillin-streptomycin (P/S) at 37°C for 4 hours. The medium was then supplemented with 10 μg/ml of purified TAT-C3 or HA-tagged C3 (HA-C3). After 24-hour incubation, the medium was removed and the cells were washed three times with 1×PBS, followed by fixation in 4% paraformaldehyde for 10 minutes. To detect the presence of intracellular C3, cells were permeabilized with 0.1% TritonX-100 for 5 minutes and blocked with 3% bovine serum albumin (BSA) in 1×PBS for 1 hour before the application of anti-HA antibody at a dilution of 1:100 in 3% BSA. Immunoreactivity was detected by anti-rabbit secondary antibodies conjugated with Alexa Fluor 488 (Molecular Probes, OR, USA) at 1:1,000 dilution. Coverslips were mounted on microscopic slides in an anti-fading solution FluorSave (Calbiochem, CA, USA). Immunofluorescence signals were examined under fluorescence microscope (Leica Microsystems, Wetzler, Germany).

To test the ability of TAT-C3 in inducing neurite outgrowth, neuroblastoma N1E-115 was plated at a density of 1×10^5 cells on 12 mm circular glass coverslips coated with laminin in 24-well culture dish and cultured in DMEM with 10% FBS at 37°C. The medium was then supplemented with purified TAT-C3 or HA-tagged C3 at a final concentration of 10 μg/ml. At fixed time point of 6, 12, and 24 hours, cells were fixed with 4% paraformaldehyde, permeabilized with 0.1% TritonX-100, and stained with TRITC-conjugated phalloidin at a concentration of 100 ng/ml to reveal actin cytoskeleton in cell body and neurites. Presence of TAT-C3 in N1E-115 cells was detected by anti-HA immunostaining as described above.

Encapsulation of TAT-C3 in PLGA Microspheres

TAT-C3 was encapsulated in PLGA microspheres by a water-in-oil-in-water (W/O/W) emulsion method adapted from Pean *et al.* (38). Briefly, TAT-C3 protein was mixed with the excipient PEG (4:1 w/w) and emulsified in dichloromethane containing 117 mg of PLGA in an ice bath, using a probe-type sonicator (XL2000, Misonix, NY, USA). This water-in-oil emulsion was then added into an external aqueous solution of PVA (5% w/v) and stirred for 1 minute on a magnetic stirrer. The resulting water-in-oil-in-water emulsion was added to de-ionized water and stirred for a further 30 minutes to extract and evaporate the organic solvent. The microspheres were then washed three times with de-ionized water and freeze-dried overnight to obtain a fine white powder, which was stored at 4°C until further analysis. Blank microspheres were prepared in the same way, but with de-ionized water as the internal aqueous phase. To evaluate the effect of polymer blends on the release profile of TAT-C3, microspheres were prepared at 100/0, 70/30, 50/50, 30/70, and 0/100 ratios of capped/uncapped PLGA. The samples were named 100/0, 70/30, 50/50, 30/70, and 0/100 respectively. Blank microspheres were also prepared in the same set of ratios.

Morphology and Encapsulation Efficiency of PLGA Microspheres

Surface morphology and internal microstructure of PLGA microspheres before and after *in vitro* degradation studies was observed using a scanning electron microscope (SEM) (JSM-5600LV, JEOL). Internal structure of microspheres was revealed by slicing freeze-dried microspheres with razor blade. The diameter of 100 microspheres was determined from SEM images using the SmileView software and the values were expressed as mean ± standard deviation.

The efficiency of TAT-C3 encapsulation in microspheres was determined using a method previously reported by Yan *et al.* (39). Briefly, a known amount of microspheres (~10 mg) was added to 0.9 N sodium hydroxide and shaken on an orbital shaker at room temperature for 4 hours. When the microspheres were solubilized completely, the resulting clear solution was neutralized to pH 7.0 by 0.9 M hydrochloric acid. The amount of TAT-C3 in the solution was determined by microBCA assay (Pierce, IL, USA) following manufacturer's instructions. Measurements were performed in triplicate and the results presented as mean ± standard deviation. Encapsulation efficiency was calculated using equation 1, by comparing the amount of protein in solubilized microspheres as detected by the microBCA assay (W_{actual}) with the amount of protein that should theoretically be present in the same amount of microspheres ($W_{theoretical}$).

$$\text{Encapsulation efficiency}(\%) = (W_{actual}/W_{theoretical}) \times 100 \quad (1)$$

In Vitro Release Profile of TAT-C3

The release profile of TAT-C3 from microspheres was determined by incubating 10 mg microspheres in 250 μl of a HEPES buffer (100 mM HEPES, pH 7.4, 10 mM NaCl) at 37°C with shaking. At predetermined time intervals, the supernatant was harvested by pelleting the microspheres at 2,000 rpm and stored at −20°C until further analysis. The amount of TAT-C3 released was determined by a novel enzyme-linked immunosorbent assay (ELISA). Briefly, TAT-C3 protein in the medium was immobilized in microplate wells (Nunc, Roskilde, Denmark) overnight at 4°C. After blocking with 1% BSA, TAT-C3 immunoreactivity was detected by anti-HA antibodies at a dilution of 1:800, followed by anti-mouse HRP antibodies (1:5,000) and ABTS substrate (Roche Diagnostics, Mannheim, Germany) in

acetate buffer. Absorbance was measured at 405 nm in a microplate reader. The amount of TAT-C3 was determined from a standard curve of known quantities of fresh TAT-C3. The value at each time interval was expressed as mean ± standard deviation.

Characterization of Microspheres Degradation *in Vitro*

Ten milligrams of blank microspheres were suspended in 250 μl of HEPES buffer and incubated at 37°C with shaking and weekly change of medium for up to 4 weeks. Microspheres of each formulation were harvested weekly in triplicate and freeze-dried for 24 hours. The degree of microspheres degradation over time was characterized by measurement of their molecular weight and residual mass, and observation of microstructure by SEM. Remaining mass of polymer was calculated according to equation 2 by comparing the mass at a given time point (W_t) to the initial mass (W_o). Measurements were performed in triplicate, and the results expressed as mean ± standard deviation.

$$\text{Percentage mass remaining} = (W_t/W_o) \times 100\% \quad (2)$$

Polymer molecular weight was determined by gel permeation chromatography on a Agilent HP 1100 LC system (Palo Alto, CA, USA) connected with the PLgel Mixed-C column and a refractive index detector. The mobile phase was tetrahydrofuran (THF). Briefly, 1 mg of microspheres was dissolved in 1 ml THF, filtered through a 0.45 μm PTFE filter, and 20 μl of it was injected and eluted with THF at 1 ml/min. Weight-average molecular weights (M_w) were calculated with polystyrene standards (Agilent, CA, USA) of molecular weight 580, 7200, 113000 and 1950000 Da, using the HPChem software. The degradation rate constant for each microsphere formulation was calculated based on the knowledge that the degradation of polyesters such as PLGA proceeds by random hydrolytic chain scission of ester linkages, which is auto-catalyzed by the carboxyl-end groups. This process may be described by first order kinetics (40). The weight average molecular weight (M_w) for each sample, at each time point, was first normalized against the initial weight average molecular weight (M_{wo}). Semi-log plots of the normalized weight average molecular weight *versus* time (in days) were plotted (data not shown). The slope was determined by a linear least squares fit to the data and expressed in units of day^{-1}. The slope represents the first-order degradation rate constant of M_w decay.

Assay of TAT-C3 Bioactivity by ADP-ribosylation of RhoA

The bioactivity of TAT-C3 protein can be assessed by its catalysis of ADP-ribosylation of RhoA, which results in an increase in molecular weight of RhoA upon Western blot analysis. A modified *in vitro* ADP-ribosylation assay (41) was used in the present study. Briefly, known amount of freshly purified TAT-C3 was serially diluted in HEPES buffer to a final volume of 50 μl and mixed with 150 μl of an assay solution containing 400 ng RhoA, 8 μM β-NAD (Roche Diagnostics, Mannheim, Germany), 5 mM $MgCl_2$, and 1 mM dithiothreitol (DTT). The reaction was incubated at 37°C for 2 hours. An aliquot of 10 μl of the reaction mixture was resolved on 10% SDS-polyacrylamide gel, followed by Western blot detection with anti-RhoA antibodies (1:500 dilution). Immunoreactivity was quantified by densitometry using a chemiluminescent imaging system (ChemiGenius2, Syngene, Maryland, USA). The extent of ADP-ribosylation was calculated using equation 3 and plotted against TAT-C3 concentrations to establish a standard curve. A linear least squares fit to the data with r^2=0.99 was obtained (data not shown).

$$\%\,\text{ADP-ribosylation} = \frac{\text{densitometric units of ADP-ribosylated RhoA}}{\text{densitometric units of total RhoA}} \times 100\% \quad (3)$$

To determine the proportion of TAT-C3 released from microspheres that remains active, 50 μl of medium harvested at various time points was added to the assay solution and subjected to Western blot analysis as described above. The amount of active TAT-C3 was then determined from the standard curve. The proportion of biologically active form of TAT-C3 relative to total amount of the protein present in the sample as determined by ELISA assay was calculated as the following:

$$\%\,\text{active TAT-C3 in medium} = \frac{\text{amount of active TAT-C3 in medium}}{\text{total amount of TAT-C3 in medium}} \times 100\% \quad (4)$$

RESULTS

TAT-C3 Efficiently Transverses Cell Membrane and Ribosylates RhoA

Accumulating evidence suggests the beneficial effect of targeted inhibition of RhoA by C3 transferase in promoting neuronal regeneration in severed CNS (24–27). The exoenzyme C3 transferase from *Clostridium botulinum* has long been known to specifically inhibit RhoA by ADP-ribosylation of its effector domain (23). The efficiency of this 24 kDa protein to enter cell, however, is very low because it lacks the cell surface binding and transport components typically found in other families of bacterial toxins. To harness its therapeutic value in promoting neuronal regeneration, an 11-amino acid protein transduction domain derived from the Tat protein of human immunodeficiency virus was engineered to the amino terminus of C3 to enhance its membrane permeability efficiency. TAT-C3 protein carrying a HA-epitope tag was expressed as a GST-fusion protein (Fig. 1A, lane *1*, 54.7 kDa) and released from the GST moiety by thrombin-mediated cleavage (Fig. 1A, lane *2*, 28.7 kDa). The cell membrane permeability of this TAT-C3 fusion protein was assessed by adding it to NIH3T3 fibroblasts at a concentration of 10 μg/ml. Immunofluorescence staining for the HA epitope on TAT-C3 six hours after incubation revealed intense intracellular signals in over 95% of the treated cells, indicating successful entry of the protein (Fig. 1B). Laser scanning confocal microscopy analysis of optical sections of cells transduced with TAT-C3 showed localization of TAT-

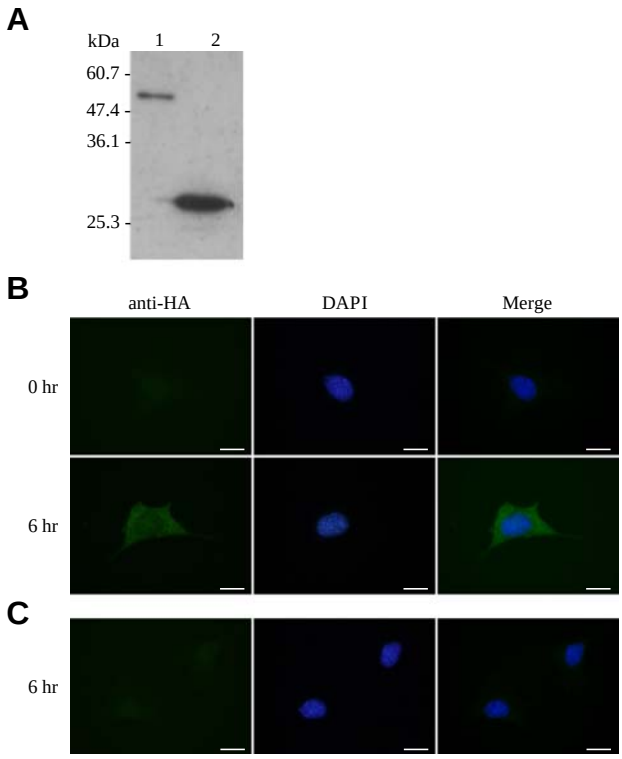

Fig. 1. Production of TAT-C3 protein and assay for its cell permeability. (**A**) Western blot analysis of TAT-C3 in the form of GST-fusion protein (lane 1) and free protein after being released from the GST moiety by thrombin cleavage (lane 2) using anti-HA antibody. NIH3T3 cells treated with TAT-C3 (**B**) or HA-tagged C3 transferase (**C**) for 6 hours were subjected to immunocytochemical staining. Anti-HA antibody binds to the HA epitope on TAT-C3 or HA-C3 (followed by detection with Alexa488-conjugated secondary antibody), whereas DAPI stains the nucleus. Scale bar = 20 μm.

C3 mainly to the cytoplasm (data not shown). Cells treated with the same concentration of HA-tagged C3 transferase showed no detectable immunofluorescence signal (Fig. 1C). While the modification of C3 transferase by TAT peptide was found to successfully enhance cell permeability of the protein, its biological activity in blocking RhoA function remains to be determined. To this end, the degree of ribosylation of intracellular RhoA by TAT-C3 was measured by Western analysis of the lysates from NIH3T3 cells treated with TAT-C3. In untreated NIH3T3 control, anti-RhoA antibodies detected a ~24 kDa band that corresponds to the endogenous wild-type RhoA protein (Fig. 2, lane *1*, arrowhead). Cells treated with TAT-C3 at 5 μg/ml showed retardation in the electrophoretic mobility of RhoA (Fig. 2, lane *2*, arrow), indicating the transfer of ADP ribose moiety to the protein by C3. The activity of TAT-C3 was further confirmed by the dose-dependent increase in population of ribosylated RhoA as its concentration in culture medium was increased from 5 to 50 μg/ml (Fig. 2, lanes *2–5*).

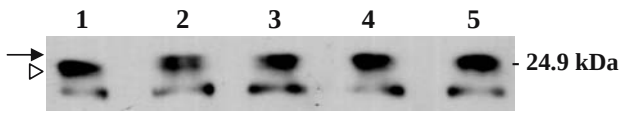

Fig. 2. Western blot analysis of endogenous RhoA in NIH3T3 cells after incubation with TAT-C3 at final concentration of 5, 10, 20, and 50 μg/ml (lanes 2 to 5). Untreated cells (lane 1) showed a 24 kDa band of wild-type RhoA (arrowhead) whereas TAT-C3 treated cells showed an additional band of higher molecular weight representing ribosylated RhoA (arrow). Bands at the bottom are non-specific signals.

TAT-C3 Promotes Neurite Outgrowth in N1E-115 Neuroblastoma

We then asked if the RhoA-inhibiting effect of TAT-C3 observed *in vitro* could be translated into cellular changes in neuronal cells. C3 transferase has previously been shown to induce formation of filopodia that resemble neurite outgrowth when microinjected into N1E-115 neuroblastoma (42), a commonly used neuronal cell line for neurite outgrowth studies (43–46). The effect is mediated through RhoA inactivation because microinjection of dominant negative $RhoA^{T19N}$ into N1E-115 cells produces the same effect (42). To evaluate the biological activity of TAT-C3 on neurons, N1E-115 neuroblastoma was cultured in medium containing 10 μg/ml TAT-C3 protein. Changes in cell morphology and actin cytoskeleton were documented at various time points. While no appreciable changes were observed in N1E-115 at 0 and 6 hours after TAT-C3 treatment (data not shown), significantly more cells exhibited outgrowth of cellular processes upon incubation in TAT-C3 medium for 12 and 24 hours (Fig. 3A) as compared to the HA-C3 (Fig. 3B) and untreated control (not shown). Further analysis revealed that over 90% of TAT-C3 positive N1E-115 displayed two or more neurites 24 hours post-treatment. These findings indicate that the modification of C3 with TAT moiety facilitates cell entry of the protein without compromising its activity in inducing neurite outgrowth by RhoA inhibition.

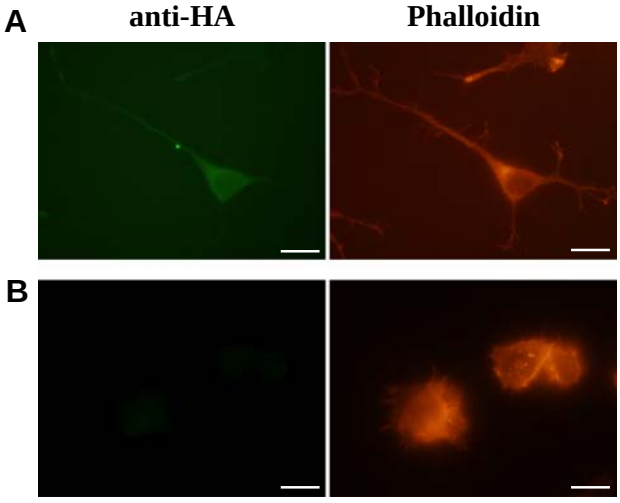

Fig. 3. Neurite outgrowth in N1E-115 neuroblastoma induced by TAT-C3. (**A**) TRITC-conjugated phalloidin decorated actin filaments in long neurites of N1E-115 treated with TAT-C3 at 10 μg/ml for 24 hours. Intracellular localization of TAT-C3 was revealed by anti-HA immunostaining using Alexa488-conjugated secondary antibody. (**B**) Anti-HA immunostaining showed no detectable signal in N1E-115 treated with HA-C3. Phalloidin stain revealed normal actin structures without major process outgrowth. Scale bar = 20 μm.

Physical Characteristics of TAT-C3 Loaded Microspheres

Having confirmed the biological activities of TAT-C3, the protein was encapsulated in various formulations of PLGA polymer to develop a microsphere-based delivery system capable of continual and steady release of the therapeutic protein. Various blends of capped and uncapped PLGA that differ in their hydrophilicity were used to modulate the protein release profile of microspheres. SEM analysis showed that the mean diameter of microspheres ranges from 74 to 85 μm, which was apparently independent of polymer formulations (Table I). The encapsulation efficiency of TAT-C3 protein in the microspheres was consistently above 80%, which also showed no major variations across different blends of polymers (Table I). SEM studies of microspheres revealed that formulations containing higher proportion of capped PLGA produced spherical microspheres with smooth and slightly porous surface (Fig. 4A–C). A rough surface and a greater level of surface porosity were observed as the proportion of uncapped PLGA reaches 70 and 100% (Fig. 4D, E). The internal microstructure of all the microspheres features spherical pores (Fig. 4F–J).

Release Profile of Encapsulated TAT-C3 from PLGA Microspheres

To characterize the release profile of encapsulated TAT-C3, microspheres of different blend ratios of capped/uncapped PLGA were incubated in HEPES buffer and the amount of TAT-C3 protein released was measured by ELISA assay. Microspheres fabricated from 100% capped PLGA (100/0) exhibited less than 10% burst release of TAT-C3 within 24 hours, followed by a lag phase of about 15 days during which only a modest level of TAT-C3 was found in the medium (Fig. 5). An ensuing gradual increase in protein release was observed, reaching a cumulative value of about 35% of total TAT-C3 encapsulated on day 28. By contrast, microspheres synthesized with 100% uncapped PLGA (0/100) showed a significant initial burst release of 40% TAT-C3 within the first 24 hours of incubation, followed by a subsequent average daily release rate of about 2.5% before a cumulative release of 80% encapsulated protein was reached by day 28 (Fig. 5). Other microspheres comprising blends of

Table I. Physical Characteristics of TAT-C3 Microspheres

Microsphere Formulation (capped/uncapped PLGA)	Microsphere Size[a] (μm)	Theoretical Loading[b] (% *w/w*)	Encapsulation Efficiency[c] (%)
100/0	83±22	0.015	84.3±0.5
70/30	85±26	0.015	80.4±2.3
50/50	76±16	0.015	87.0±1.3
30/70	75±16	0.015	84.8±1.6
0/100	74±18	0.015	82.5±2.0

[a] Values are given as mean ± standard deviation of 100 representative microspheres in each formulation.
[b] Theoretical loading was calculated as the percentage (w/w) of TAT-C3 per dry weight of microspheres.
[c] Values are mean ± standard deviation of three measurements for each formulation.

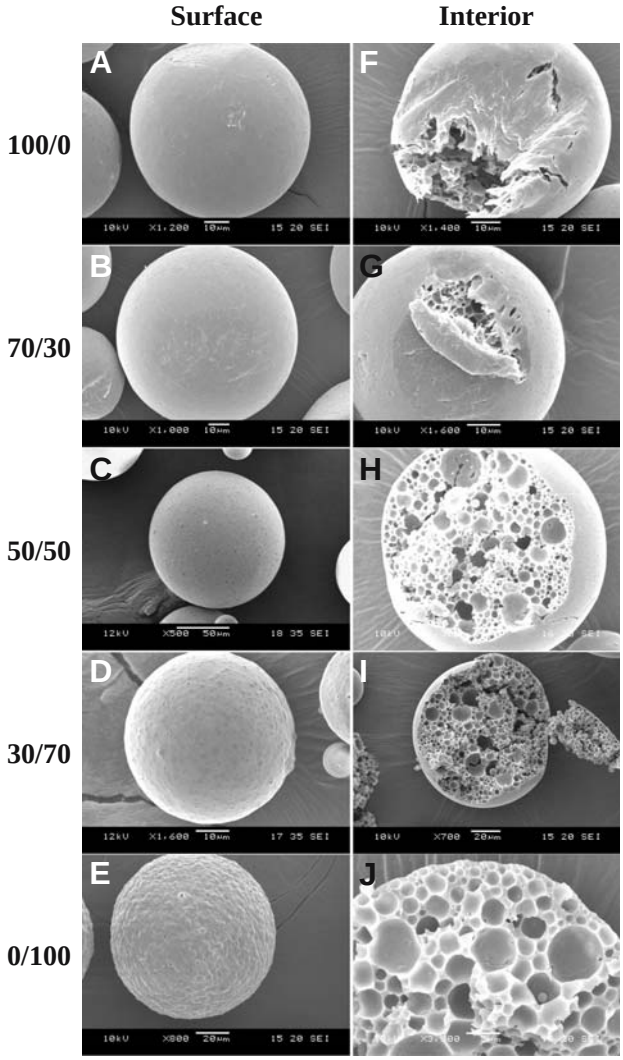

Fig. 4. Scanning electron micrographs of microspheres prepared from different blends of capped/uncapped PLGA to show surface morphology (A–E) and internal microstructure (F–J).

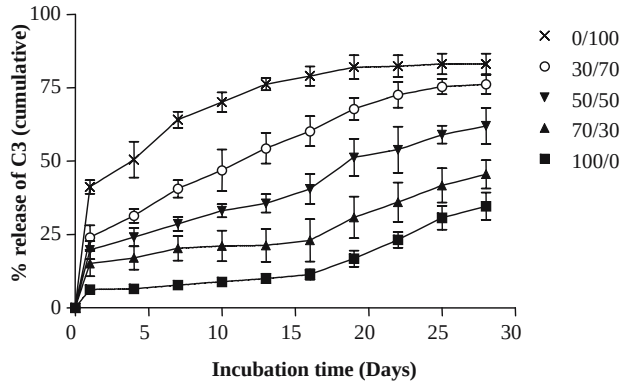

Fig. 5. Cumulative release of TAT-C3 from microspheres of different blends of capped and uncapped PLGA. The amount of TAT-C3 released was determined by ELISA assay and expressed as percentage of total protein encapsulated. Error bars represent mean ± standard deviation from triplicates.

capped/uncapped PLGA at various ratios were found to exhibit release profiles intermediate between the two extremes. Importantly, the undesirable initial burst release of protein was dampened as the proportion of capped PLGA in the microspheres was increased. In fact, former studies of PLGA microspheres suggested the initial burst release was at least partially attributable to the immediate dissolution and release of proteins near the surface of microspheres (47–49). It is plausible that the prominent initial burst within the first 24 hours in the 0/100 formulation was partly contributed by the rough surface of the microspheres, which conferred a large surface area exposing to aqueous environment, thereby increasing the rate and extent of initial hydration of the microspheres (47). Microspheres fabricated with higher capped PLGA content have smooth surface (Fig. 4A–D), which might have helped to attenuate the degree of initial burst. Further, the lag period of protein release is gradually eliminated as the level of uncapped polymer is raised (Fig. 5). Among the formulations tested, the 30/70 blend in particular shows a mild initial burst of 25%, while still maintaining a subsequent average daily release of 2.3% encapsulated protein (Fig. 5). This translates to an average release rate of 3 ng TAT-C3 per mg microspheres per day over a period of one month.

Physical Changes of TAT-C3 Encapsulated PLGA Microspheres During *In Vitro* Degradation

Protein drugs encapsulated in PLGA microspheres are released into the milieu via diffusion through interconnected channels that are formed during polymer degradation and erosion (48). To study the effect of uncapped and capped PLGA on the degradation and erosion characteristics of microspheres, and hence on the release kinetics of TAT-C3, the molecular weight, mass loss, and morphology of microspheres were monitored throughout the course of *in vitro* incubation in HEPES buffer.

The molecular weight of the 100/0 formulation drops by less than 3% during the first week (Fig. 6A). This slow rate of degradation explains the modest degree of mass loss during this period (Fig. 6B). These observations were in line with findings from SEM analysis of the 100/0 microspheres, which maintained spherical shape and structural integrity (Fig. 7, *100/0*). No major morphological changes in microspheres were observed until the end of second week, during which a slightly rougher and porous surface was observed, suggesting a mild degree of surface erosion (Fig. 7, *100/0*). The lack of any significant degradation during the first three weeks of incubation accounts for the initial lag period of minimal TAT-C3 release. The more discernible surface erosion of microspheres found on day 21 coincided with an increase in the release rate of TAT-C3 (Fig. 5). The overall triphasic (S-type) release profile is consistent with the typical release kinetics of other protein drugs encapsulated in PLGA polymer (50,51).

In contrast, microspheres prepared from pure uncapped PLGA (0/100) exhibited faster release kinetics. The molecular weight decreased by almost 30% within the first week of incubation (Fig. 6A), which is consistent with that reported in another study (52). Taking into consideration the continuous loss of mass in the 0/100 microspheres starting from the early

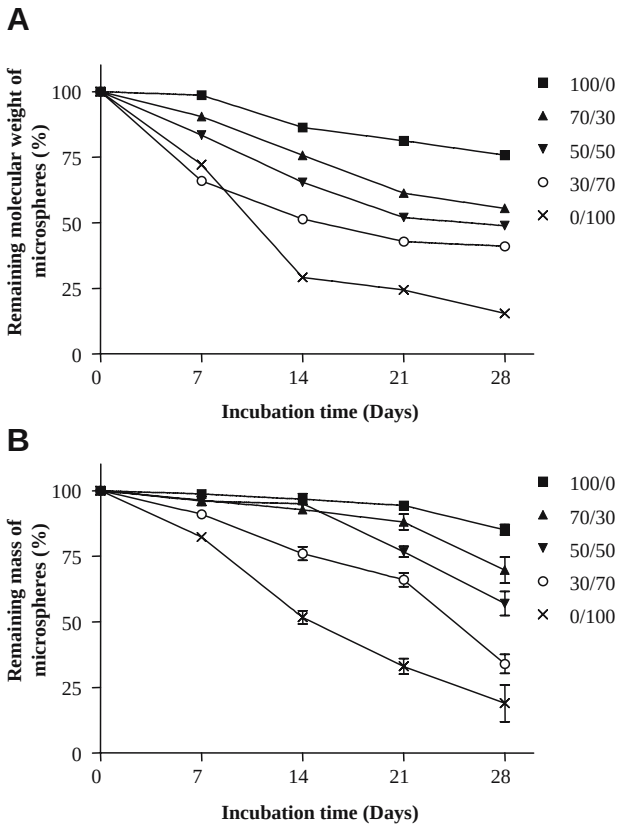

Fig. 6. (**A**) Change in weight-average molecular weight of microspheres incubated in HEPES buffer. The values were expressed as percentage of initial molecular weight. (**B**) Mass loss profile of microspheres incubated in HEPES buffer. The values were expressed as percentage of initial mass. Error bars represent mean ± standard deviation from triplicates.

phase of incubation (Fig. 6B), it is speculated that the instantaneous solubilization of PLGA degradation products expedites the erosion process in this blend of microspheres. This conjecture is corroborated by morphological changes observed in the degrading microspheres, which show deformation and increased surface porosity within the first week of incubation (Fig. 7, *0/100*). The higher degradation rate of the 0/100 microspheres ($-0.0688\ \text{day}^{-1}$) compared to that of the 100/0 microspheres ($-0.0107\ \text{day}^{-1}$) is therefore not surprising. Faster degradation of uncapped PLGA can be attributed to its high hydrophilicity, which leads to more water uptake and extensive hydrolysis of ester bonds in large number of free carboxyl end groups in this polymer (53), making the microspheres increasingly fragmented and porous over time. The ongoing erosion process upon incubation in medium leads to the continuous release of TAT-C3 protein.

Our results demonstrated that blending capped and uncapped PLGA polymers at various proportions yielded microspheres with degradation kinetics intermediate between the two pure formulations. In fact, an increase in the proportion of uncapped polymer led to higher rate of degradation and mass loss of microspheres. The progression of pore formation and microsphere fragmentation was also hastened. For all the blends examined, the time point at which a significant mass loss begins correlates well with an increase in the rate of TAT-C3 release from microspheres.

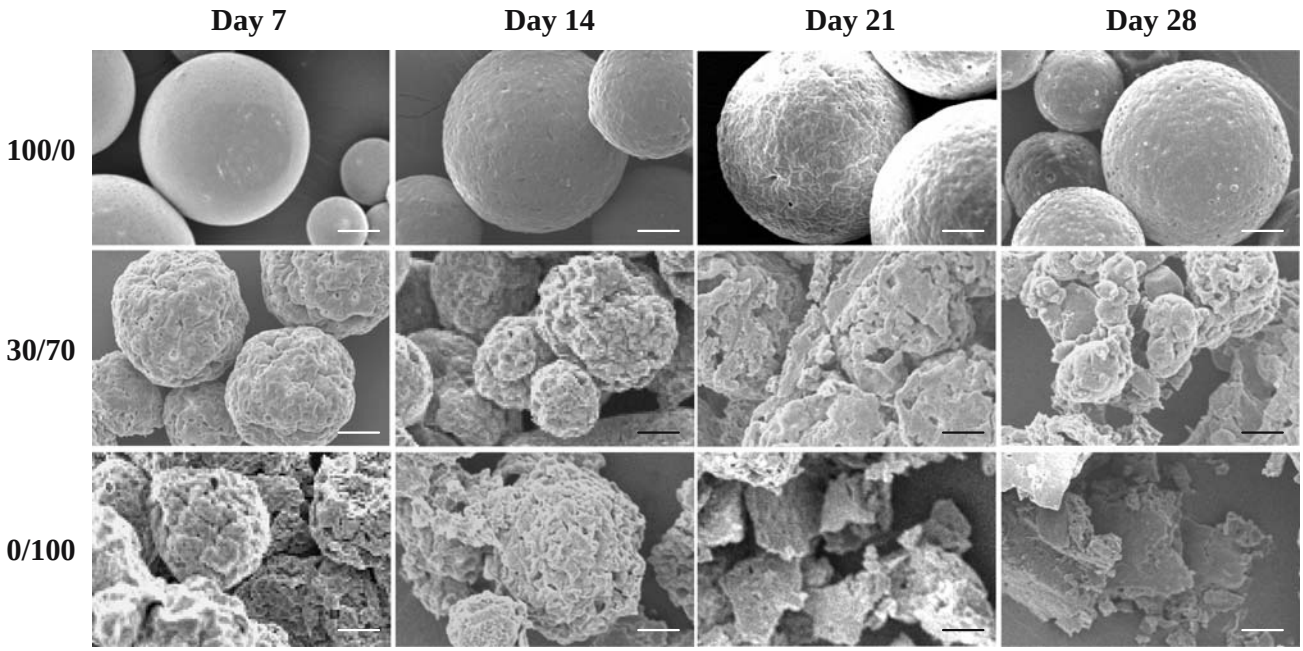

Fig. 7. Scanning EM images to show surface morphology of microspheres over the 1-month incubation period. Scale bar = 20 μm.

Interestingly, analysis of cross section of the 30/70 microspheres after 7 days of incubation revealed the presence of newly formed internal pores on the wall of existing pores, which form a network of interconnected channels within the microspheres (Fig. 8). Such pores were not observed in the cross section of microspheres prior to incubation. Similar observation was made for the 50/50 and the 70/30 microspheres at a later time point on day 14 (data not shown). There is evidence that even in a homogenous mixture of two polymers, gelling and solidification of the polymers occur separately (54). Based on this, we hypothesized that the new pores observed on walls of existing pores arose because the more hydrated domains of uncapped polymer within microsphere matrix degraded and eroded first. Gradual formation of a network of interconnected channels facilitated the escape of polymer degradation products into the medium, and hence the release of encapsulated TAT-C3 via diffusion. Variations in proportion of capped and uncapped PLGA in microspheres may therefore alter the abundance of these channels and hence the release profile of encapsulated proteins. The presence of these interconnected channels in the 30/70 microspheres in early period of incubation may account for the elimination of initial lag, yet maintain sustained release of TAT-C3 throughout the course of study.

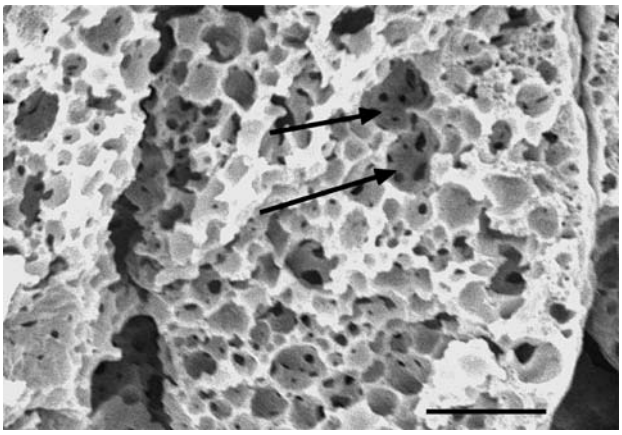

Fig. 8. Scanning EM analysis of internal structure of the 30/70 blend microspheres after 7 days of incubation in HEPES buffer. Arrows indicate some of the newly formed farnestrations on wall of the existing pores, leading to formation of interconnected channels within the microsphere. Scale bar = 10 μm.

Bioactivity of TAT-C3 Transferase Released from PLGA Microspheres

One of the major concerns in using polymeric microspheres as depot for sustained and controlled release of therapeutic proteins is the preservation of their bioactivities. To measure the activity of TAT-C3 released from PLGA microspheres, conditioned medium was harvested at various time points and subjected to *in vitro* ADP-ribosylation assay using recombinant RhoA as substrate. By interpolation of a standard curve established with fresh C3 transferase, the amount of active TAT-C3 in the medium was determined and expressed as a percentage of the total TAT-C3 released (as detected by ELISA) (Fig. 9). For the 30/70 blend, which shows optimal release kinetics among other formulations tested, around 70% of TAT-C3 released on the first day of incubation was found active. Since the microspheres have been exposed to medium for just 24 hours, the partial loss of protein activity may be attributed to the compromised TAT-C3 protein integrity during the microencapsulation process. Mechanical stress introduced by sonication steps during microsphere fabrication, for instance, has been reported to cause protein degradation (55,56). Further, protein adsorption to the aqueous-organic interface during formation of the first water-in-oil emulsion can contribute to protein inactivation and aggregation (57,58). The inclusion of excipients such as PEG and BSA in the first aqueous phase have been found

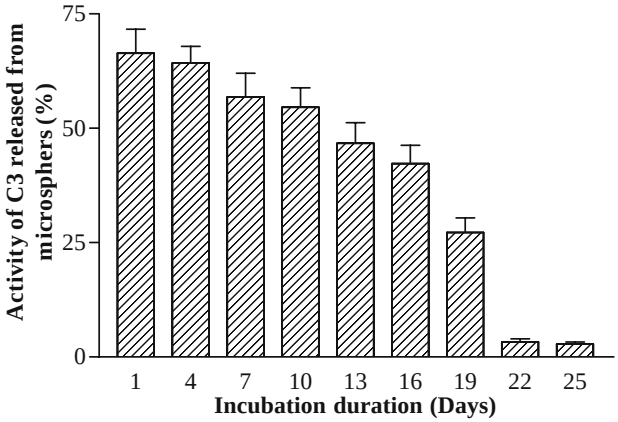

Fig. 9. Percentage of active TAT-C3 released from the 30/70 microspheres. The amount of active TAT-C3 in each sample was determined by RhoA ribosylation assay and expressed as percentage of total TAT-C3 encapsulated in the microspheres. Data were expressed as mean ± standard deviation from triplicates.

to reduce these compromise in protein activities (38,59). The preservation of TAT-C3 activity in the 30/70 blend is attributable to the protective effect of PEG against the protein-denaturing organic solvent during primary emulsification process. In the ensuing 14 days of *in vitro* incubation, 50–60% of TAT-C3 protein released from the microspheres still remained active in ribosylating RhoA. Nonetheless, the level fell to 30% on day 19, followed by a precipitous drop towards day 22. By contrast, free TAT-C3 incubated under the same conditions exhibited a much faster drop to below 10% of residual RhoA ribosylation activity as early as day 13 of incubation (data not shown). This observation led to our speculation that TAT-C3 encapsulated in PLGA microspheres is partially protected against inactivation, possibly through protein-PLGA/PEG interactions that reduce protein aggregation and unfolding as in the case of free protein in solution. Nonetheless, this holds only when the structure of microspheres still remains intact. When the blend 30/70 starts to lose structural integrity towards day 21 (Fig. 7), it is accompanied by a drastic drop in TAT-C3 activity (Fig. 9).

DISCUSSION

Accumulating evidence points to the pivotal role of RhoA activation in various counter-regeneration events in severed mammalian CNS. To exploit the therapeutic potential of the potent RhoA inhibitor C3 transferase, which shows low efficiency of cell entry, we fused the Tat transduction domain of human immunodeficiency virus to its amino terminus. Immunostaining results showed that the resulting TAT-C3 protein entered cells as early as 6 hours after incubation and remained active in inhibiting RhoA through ADP-ribosylation, which corroborates findings in previous reports using similar proteins (60–63). In this study, the blending of polymers with hydrophobic ester end-groups (capped PLGA) and hydrophilic carboxyl end-groups (uncapped PLGA) was demonstrated to be an effective method of controlling the release characteristics of TAT-C3. For all the blends tested, there is always a good correlation in timing between the increase in rate of release of TAT-C3 and the physical erosion of microspheres. This indicates that the release of TAT-C3 from the microspheres is erosion-controlled. In particular, the 30/70 blend of capped/uncapped PLGA was found to be the optimal formulation that allows a continuous release of TAT-C3 upon incubation of the microspheres in buffer. Following the initial burst of 25% on day 1, TAT-C3 release was maintained at an average daily rate of 3 ng/day/mg microspheres up to the end of study on day 28 as determined by ELISA assay. The initial burst release of TAT-C3 at this level in fact can be advantageous in its application in treating spinal injuries because evidence suggests that administering a large dose of C3 transferase to injured CNS tissue within the first 24 hours after injury provides neuroprotective effects (24). This is at least partially attributable to the anti-apoptotic effect of C3. Previous findings suggested that both neurons and glia in the spinal cord undergo apoptosis as early as the first day after traumatic injury, which leads to subsequent formation of a large lesion cavity in the severed cord and impedes axonal regeneration (64–66). Preventing death and maintaining survival of neurons and oligodendrocytes in the early phases of spinal injury is therefore important for the ensuing functional recovery. C3 transferase treatment has been shown to significantly reduce the apoptotic population of neurons and glia (67). The peculiar release profile of mild initial burst of TAT-C3 in this PLGA formulation is expected to cater to the anti-apoptotic need in the initial phase of spinal injury treatment. Further, the subsequent steady release of TAT-C3 from this blend of PLGA microspheres promises a continual supply of the therapeutic protein to suppress RhoA signaling triggered by various myelin inhibitors that block neuronal regeneration. This PLGA-based depot system therefore helps to reduce cell death while counteracting effects of myelin inhibitor. By combining with other treatments such as supplement of nerve growth factor and anti-inflammatory agents at the site of injury, a microenvironment that favors long-distance axonal regeneration of injured neurons is warranted.

With regard to stability of protein in microspheres, the finding that 70% of TAT-C3 released from microspheres on the first day of incubation is biologically active suggests the encapsulation protocol preserves the integrity of protein. The fraction of biologically active TAT-C3 released in the first three weeks of incubation is still within acceptable levels. From day 22 onward however, a precipitous drop in the activity of TAT-C3 was observed. In fact, similar findings of low biological activities in encapsulated protein have been reported when microspheres are incubated in a fixed volume of buffer in a closed container (68,69). The loss of protein integrity during incubation of microspheres *in vitro* can be attributed to a number of reasons, such as protein aggregation following initial re-hydration of the microspheres, protein adsorption to the polymer, or protein denaturation due to acidification of the medium by PLGA degradation products (70,71). The use of HEPES buffer in this study indeed minimizes the problem of acidification because of its stronger buffer capacity than phosphate-buffered saline. The harvest of incubation medium for TAT-C3 activity assays every three days also ensures the maintenance of medium at neutral pH throughout the course of study (data not shown).

Upon prolonged incubation at 37°C, however, the increasing porosity and hydration of microspheres over time exposes the encapsulated TAT-C3 to chemical stress and renders the protein unstable. Taking into account the concurrence of heightened deterioration of TAT-C3 activity and the massive structural degradation of PLGA microspheres after the third week of incubation, it is plausible that the polymer degradation products at this stage comprises of an overwhelming proportion of soluble monomers and oligomers that compromise the stability of TAT-C3. These degradation species may exert co-solvent effects on TAT-C3 that reduces protein conformational stability (70). When TAT-C3 microspheres are applied to the severed spinal cord however, these polymer degradation products are expected to be readily scavenged by microglia and infiltrating neutrophils, thereby minimizing their detrimental effects on the biological activities of TAT-C3 released (72,73). Discrepancy between the amount of TAT-C3 released (ELISA assay) and the activity of TAT-C3 in the medium indicates a minimal loss of C3 immunoreactivity but significant compromise in its biological activity. There is evidence from previous studies (70,74–76) that antigen reactivity may not be strictly related to biological activity because a protein may lose biological activity without losing its epitope reactivity.

CONCLUSION

This study demonstrated the enhancement of cell permeability of C3 transferase by the Tat transduction domain of human HIV without compromising its biological activity. To harness this promising therapeutic agent in treating spinal injuries, we tested the feasibility of developing a biopolymer-based depot system for sustained release of TAT-C3 *in vivo*. Using the w/o/w emulsification method and PEG as excipient, TAT-C3 was successfully encapsulated in biocompatible PLGA polymer in the form of microspheres and 70% of its activity was preserved during the fabrication process. By adjusting the ratio of capped and uncapped PLGA, an optimal blend that allows mild initial burst, subsequent gradual and continual release of biologically active TAT-C3 was established. Given the pivotal role of RhoA in myelin and glial scar inhibitory pathways, as well as its implication in apoptosis during CNS injury, this therapeutics delivery system will find its application in spinal injury and stroke treatment. Importantly, protein encapsulated PLGA microspheres can be freeze-dried for long-term storage and easily re-dispersed in aqueous solutions (77), ensuring their readily availability. Assessment of the efficacy of this TAT-C3 microsphere depot system in promoting function recovery in animal models of CNS injuries is underway. This system is expected to complement depot system of neurotrophic factors and nerve conduit in promoting CNS regeneration.

REFERENCES

1. E. Emery, P. Aldana, M. B. Bunge, W. Puckett, A. Srinivasan, R. W. Keane, J. Bethea, and A. D. Levi. Apoptosis after traumatic human spinal cord injury. *J. Neurosurg.* **89**:911–920 (1998).
2. M. J. Crowe, J. C. Bresnahan, S. L. Shuman, J. N. Masters, and M. S. Beattie. Apoptosis and delayed degeneration after spinal cord injury in rats and monkeys. *Nat. Med.* **3**:73–76 (1997).
3. S. Casha, W. R. Yu, and M. G. Fehlings. Oligodendroglial apoptosis occurs along degenerating axons and is associated with FAS and p75 expression following spinal cord injury in the rat. *Neuroscience* **103**:203–218 (2001).
4. S. Ramon y Cajal. *Degeneration and regeneration of the nervous system*, Oxford University Press, London, 1928.
5. M. Berry. Post-injury myelin-breakdown products inhibit axonal growth: a hypothesis to explain the failure of axonal regeneration in the mammalian central nervous system. *Bibl. Anat.* **23**:1–11 (1982).
6. P. Caroni and M. E. Schwab. Two membrane protein fractions from rat central myelin with inhibitory properties for neurite growth and fibroblast spreading. *J. Cell Biol.* **106**:1281–1288 (1988).
7. M. Domeniconi and M. T. Filbin. Overcoming inhibitors in myelin to promote axonal regeneration. *J. Neurol. Sci.* **233**:43–47 (2005).
8. K. C. Wang, J. A. Kim, R. Sivasankaran, R. Segal, and Z. He. P75 interacts with the Nogo receptor as a co-receptor for Nogo, MAG and Omgp. *Nature* **420**:74–78 (2002).
9. F. J. Liuzzi and R. J. Lasek. Astrocytes block axonal regeneration in mammals by activating the physiological stop pathway. *Science* **237**:642–645 (1987).
10. P. J. Reier, L. J. Stensaas, and L. Guth. The astrocytic scar as an impediment to regeneration in the central nervous system. In C. C. Kao, R. P. Bunge, and P. J. Reier (eds.), *Spinal cord reconstruction*, Raven, New York, 1983, pp. 163–195.
11. R. A. Asher, D. A. Morgenstern, P. S. Fidler, K. H. Adcock, A. Oohira, J. E. Braistead, J. M. Levine, R. U. Margolis, J. H. Rogers, and J. W. Fawcett. Neurocan is upregulated in injured brain and in cytokine-treated astrocytes. *J. Neurosci.* **20**:2427–2438 (2000).
12. R. A. Asher, D. A. Morgenstern, M. C. Shearer, K. H. Adcock, P. Pesheva, and J. W. Fawcett. Versican is upregulated in CNS injury and is a product of oligodendrocyte lineage cells *J. Neurosci.* **22**:2225–2236 (2002).
13. M. T. Fitch and J. Silver. Activated macrophages and the blood–brain barrier: inflammation after CNS injury leads to increases in putative inhibitory molecules. *Exp. Neurol.* **148**:587–603 (1997).
14. R. A. Asher, D. A. Morgenstern, L. D. Moon, and J. W. Fawcett. Chondroitin sulphate proteoglycans: inhibitory components of the glial scar. *Prog. Brain Res.* **132**:611–619 (2001).
15. D. A. Morgenstern, R. A. Asher, and J. W. Fawcett. Chondroitin sulphate proteoglycans in the CNS injury response. *Prog. Brain Res.* **137**:313–332 (2002).
16. Y. Zhang, J. K. Winterbottom, M. Schachner, A. R. Lieberman, and P. N. Anderson. Tenascin-C expression and axonal sprouting following injury to the spinal dorsal columns in the adult rat. *J. Neurosci. Res.* **49**:433–450 (1997).
17. F. De Winter, M. Oudega, A. J. Lankhorst, F. P. Hamers, B. Blits, M. J. Ruitenberg, R. J. Pasterkamp, W. H. Gispen, and J. Verhaagen. Injury-induced class 3 semaphorin expression in the rat spinal cord. *Exp. Neurol.* **175**:61–75 (2002).
18. R. J. Pasterkamp, P. N. Anderson, and J. Verhaagen. Peripheral nerve injury fails to induce growth of lesioned ascending dorsal column axons into spinal cord scar tissue expressing the axon repellent Semaphorin3A. *Eur. J. Neurosci.* **13**:457–471 (2001).
19. C. Moreau-Fauvarque, A. Kumanogoh, E. Camand, C. Jaillard, G. Barbin, I. Boquet, C. Love, E. Y. Jones, H. Kikutani, C. Lubetzki, I. Dusart, and A. Chedotal. The transmembrane semaphorin Sema4D/CD100, an inhibitor of axonal growth, is expressed on oligodendrocytes and upregulated after CNS lesion. *J. Neurosci.* **23**:9229–9239 (2003).
20. P. P. Monnier, A. Sierra, J. M. Schwab, S. Henke-Fahle, and B. K. Mueller. The Rho/ROCK pathway mediates neurite growth-inhibitory activity associated with the chondroitin sulfate proteoglycans of the CNS glial scar. *Mol. Cell. Neurosci.* **22**:319–330 (2003).
21. V. Perrot, J. Vazquez-Prado, and J. S. Gutkind. Plexin B regulates Rho through the guanine nucleotide exchange factors leukemia-associated Rho GEF (LARG) and PDZ-RhoGEF. *J. Biol. Chem.* **277**:43115–43120 (2002).
22. J. M. Swiercz, R. Kuner, J. Behrens, and S. Offermanns. Plexin-B1 directly interacts with PDZ-RhoGEF/LARG to regulate RhoA and growth cone morphology. *Neuron* **35**:51–63 (2002).

23. E. J. Rubin, D. M. Gill, P. Boquet, and M. R. Popoff. Functional modification of a 21-kilodalton G protein when ADP-ribosylated by exoenzyme C3 of Clostridium botulinum. *Mol. Cell Biol.* **8**:418–426 (1988).
24. P. Dergham, B. Ellezam, C. Essagian, H. Avedissian, W. D. Lubell, and L. McKerracher. Rho signaling pathway targeted to promote spinal cord repair. *J. Neurosci.* **22**:6570–6577 (2002).
25. A. E. Fournier, B. T. Takizawa, and S. M. Strittmatter. Rho kinase inhibition enhances axonal regeneration in the injured CNS. *J. Neurosci.* **23**:1416–1423 (2003).
26. Z. Jin and S. M. Strittmatter. Rac1 mediates collapsin-1-induced growth cone collapse. *J. Neurosci.* **17**:6256–6263 (1997).
27. M. Lehmann, A. Fournier, I. Selles-Navarro, P. Dergham, A. Sebok, N. Leclerc, G. Tigyi, and L. McKerracher. Inactivation of Rho signaling pathway promotes CNS axon regeneration *J. Neurosci.* **19**:7537–7547 (1999).
28. B. Niederost, T. Oertle, J. Fritsche, R. A. McKinney, and C. E. Bandtlow. Nogo-A and myelin-associated glycoprotein mediate neurite growth inhibition by antagonistic regulation of RhoA and Rac1. *J. Neurosci.* **22**:10368–10376 (2002).
29. A. D. Frankel and C. O. Pabo. Cellular uptake of the tat protein from human immunodeficiency virus. *Cell* **55**:1189–1193 (1988).
30. M. Green and P. M. Loewenstein. Autonomous functional domains of chemically synthesized human immunodeficiency virus tat trans-activator protein. *Cell* **55**:1179–1188 (1988).
31. S. Fawell, J. Seery, Y. Daikh, C. Moore, L. L. Chen, B. Pepinsky, and J. Barsoum. Tat-mediated delivery of heterologous proteins into cells. *Proc. Natl. Acad. Sci. U. S. A* **91**:664–668 (1994).
32. S. Conrad, H. J. Schluesener, K. Trautmann, N. Joannin, R. Meyermann, and J. M. Schwab. Prolonged lesional expression of RhoA and RhoB following spinal cord injury. *J. Comp. Neurol.* **487**:166–175 (2005).
33. C. Brabeck, M. Mittelbronn, K. Bekure, R. Meyermann, H. J. Schluesener, and J. M. Schwab. Effect of focal cerebral infarctions on lesional RhoA and RhoB expression. *Arch. Neurol.* **60**:1245–1249 (2003).
34. J. P. Benoit, N. Faisant, M. C. Venier-Julienne, and P. Menei. Development of microspheres for neurological disorders: from basics to clinical applications. *J. Control. Release* **65**:285–296 (2000).
35. D. F. Emerich, M. A. Tracy, K. L. Ward, M. Figueiredo, R. Qian, C. Henschel, and R. T. Bartus. Biocompatibility of poly (DL-lactide-co-glycolide) microspheres implanted into the brain. *Cell Transplant.* **8**:47–58 (1999).
36. P. Menei, V. Daniel, C. Montero-Menei, M. Brouillard, A. Pouplard-Barthelaix, and J. P. Benoit. Biodegradation and brain tissue reaction to poly(D,L-lactide-co-glycolide) microspheres. *Biomaterials* **14**:470–478 (1993).
37. K. L. Guan and J. E. Dixon. Eukaryotic proteins expressed in Escherichia coli: an improved thrombin cleavage and purification procedure of fusion proteins with glutathione S-transferase. *Anal. Biochem.* **192**:262–267 (1991).
38. J. M. Pean, F. Boury, M. C. Venier-Julienne, P. Menei, J. E. Proust, and J. P. Benoit. Why does PEG 400 co-encapsulation improve NGF stability and release from PLGA biodegradable microspheres?. *Pharm. Res.* **16**:1294–1299 (1999).
39. C. Yan, J. H. Resau, M. West, W. L. Rill, and M. Kende. Characterization and morphological analysis of protein-loaded poly(lactide-co-glycolide) microparticles prepared by water-in-oil-in-water emulsion technique. *J. Control. Release* **32**:231–241 (1994).
40. E. P. Magre and A. P. Sam. Hydrolytic degradation of PLAGA, calculation of rate constants from various types of *in-vitro* degradation curves. *J. Control. Release* **48**:318–320 (1997).
41. S. T. Dillon and L. A. Feig. Purification and assay of recombinant C3 transferase. *Methods Enzymol.* **256**:174–184 (1995).
42. R. Kozma, S. Sarner, S. Ahmed, and L. Lim. Rho family GTPases and neuronal growth cone remodelling: relationship between increased complexity induced by Cdc42Hs, Rac1, and acetylcholine and collapse induced by RhoA and lysophosphatidic acid. *Mol. Cell Biol.* **17**:1201–1211 (1997).
43. Y. Kloog, J. Axelrod, and I. Spector. Protein carboxyl methylation increases in parallel with differentiation of neuroblastoma cells. *J. Neurochem.* **40**:522–529 (1983).
44. H. Li, H. C. Chen, and F. L. Huang. Identification of a rapidly dephosphorylating 95-kDa protein as elongation factor 2 during 8-Br-cAMP treatment of N1E115 neuroblastoma cells. *Biochem. Biophys. Res. Commun.* **217**:131–137 (1995).
45. T. Ishii, E. Satoh, and M. Nishimura. Integrin-linked kinase controls neurite outgrowth in N1E-115 neuroblastoma cells. *J. Biol. Chem.* **276**:42994–43003 (2001).
46. J. Yamauchi, Y. Miyamoto, A. Sanbe, and A. Tanoue. JNK phosphorylation of paxillin, acting through the Rac1 and Cdc42 signaling cascade, mediates neurite extension in N1E-115 cells. *Exp. Cell Res.* **312**:2954–2961 (2006).
47. C. G. Pitt, M. M. Gratzl, G. L. Kimmel, J. Surles, and A. Schindler. Aliphatic polyesters II. The degradation of poly (DL-lactide), poly (epsilon-caprolactone), and their copolymers *in vivo*. *Biomaterials* **2**:215–220 (1981).
48. N. Faisant, J. Siepmann, and J. P. Benoit. PLGA-based microparticles: elucidation of mechanisms and a new, simple mathematical model quantifying drug release. *Eur. J. Pharm. Sci.* **15**:355–366 (2002).
49. J. Wang, B. M. Wang, and S. P. Schwendeman. Characterization of the initial burst release of a model peptide from poly(D,L-lactide-co-glycolide) microspheres. *J. Control. Release* **82**:289–307 (2002).
50. J. M. Pean, M. C. Venier-Julienne, F. Boury, P. Menei, B. Denizot, and J. P. Benoit. NGF release from poly(D,L-lactide-co-glycolide) microspheres. Effect of some formulation parameters on encapsulated NGF stability. *J. Control. Release* **56**: 175–187 (1998).
51. C. Sturesson and J. Carlfors. Incorporation of protein in PLG-microspheres with retention of bioactivity. *J. Control. Release* **67**:171–178 (2000).
52. W. Friess and M. Schlapp. Modifying the release of gentamicin from microparticles using a PLGA blend. *Pharm. Dev. Technol.* **7**:235–248 (2002).
53. M. A. Tracy, K. L. Ward, L. Firouzabadian, Y. Wang, N. Dong, R. Qian, and Y. Zhang. Factors affecting the degradation rate of poly(lactide-co-glycolide) microspheres *in vivo* and *in vitro*. *Biomaterials* **20**:1057–1062 (1999).
54. W. I. Li, K. W. Anderson, R. C. Mehta, and P. P. Deluca. Prediction of solvent removal profile and effect on properties for peptide-loaded PLGA microspheres prepared by solvent extraction/ evaporation method. *J. Control. Release* **37**:199–214 (1995).
55. J. L. Cleland and A. J. Jones. Stable formulations of recombinant human growth hormone and interferon-gamma for microencapsulation in biodegradable microspheres. *Pharm. Res.* **13**:1464–1475 (1996).
56. M. Wolf, M. Wirth, F. Pittner, and F. Gabor. Stabilisation and determination of the biological activity of L-asparaginase in poly(D,L-lactide-co-glycolide) nanospheres. *Int. J. Pharm.* **256**:141–152 (2003).
57. M. Morlock, H. Koll, G. Winter, and T. Kissel. Microencapsulation of rh-erythropoietin, using biodegradable poly(,-lactide-co-glycolide): protein stability and the effects of stabilizing excipients. *Eur. J. Pharm. Biopharm.* **43**:29–36 (1997).
58. H. Sah. Stabilization of proteins against methylene chloride/ water interface-induced denaturation and aggregation. *J. Control. Release* **58**:143–151 (1999).
59. C. Perez-Rodriguez, N. Montano, K. Gonzalez, and K. Griebenow. Stabilization of alpha-chymotrypsin at the CH2Cl2/water interface and upon water-in-oil-in-water encapsulation in PLGA microspheres. *J. Control. Release.* **89**:71–85 (2003).
60. E. Sahai and M. F. Olson. Purification of TAT-C3 Exoenzyme. In W. E. Balch, C. J. Der, and A. Hall (eds.), *Methods in Enzymology—Regulators and Effectors of Small GTPases: Rho Family*, Academic Press, 2006, pp. 128–140.
61. J. Park, J. S. Kim, K. C. Jung, H. J. Lee, J. I. Kim, J. Kim, J. Y. Lee, J. B. Park, and S. Y. Choi. Exoenzyme Tat-C3 inhibits association of zymosan particles, phagocytosis, adhesion, and complement binding in macrophage cells. *Mol. Cells* **16**:216–223 (2003).
62. V. Sauzeau, E. MellionnecLe, J. Bertoglio, E. Scalbert, P. Pacaud, and G. Loirand. Human urotensin II-induced contraction and arterial smooth muscle cell proliferation are mediated by RhoA and Rho-kinase. *Circ. Res.* **88**:1102–1104 (2001).
63. G. Gadea, Y. Boublik, S. Delga, and P. Roux. Efficient production of Clostridium botulinum exotoxin C3 in bacteria: a

screening method to optimize production yields. *Protein Expr. Purif.* **40**:164–168 (2005).
64. X. Z. Liu, X. M. Xu, R. Hu, C. Du, S. X. Zhang, J. W. McDonald, H. X. Dong, Y. J. Wu, G. S. Fan, M. F. Jacquin, C. Y. Hsu, and D. W. Choi. Neuronal and glial apoptosis after traumatic spinal cord injury. *J. Neurosci.* **17**:5395–5406 (1997).
65. S. L. Shuman, J. C. Bresnahan, and M. S. Beattie. Apoptosis of microglia and oligodendrocytes after spinal cord contusion in rats. *J. Neurosci. Res.* **50**:798–808 (1997).
66. S. D. Grossman, L. J. Rosenberg, and J. R. Wrathall. Temporal–spatial pattern of acute neuronal and glial loss after spinal cord contusion. *Exp. Neurol.* **168**:273–282 (2001).
67. C. I. Dubreuil, M. J. Winton, and L. McKerracher. Rho activation patterns after spinal cord injury and the role of activated Rho in apoptosis in the central nervous system. *J. Cell Biol.* **162**:233–243 (2003).
68. I. J. Castellanos, R. Crespo, and K. Griebenow. Poly(ethylene glycol) as stabilizer and emulsifying agent: a novel stabilization approach preventing aggregation and inactivation of proteins upon encapsulation in bioerodible polyester microspheres. *J. Control. Release* **88**:135–145 (2003).
69. A. Aubert-Pouessel, M. C. Venier-Julienne, A. Clavreul, M. Sergent, C. Jollivet, C. N. Montero-Menei, E. Garcion, D. C. Bibby, P. Menei, and J. P. Benoit. *In vitro* study of GDNF release from biodegradable PLGA microspheres. *J. Control. Release* **95**:463–475 (2004).
70. S. P. Schwendeman, M. Cardamone, M. R. Brandon, A. Kilbanov, and R. Langer. Stability of proteins and their delivery from biodegradable polymer microspheres. In *Microparticulate systems for the delivery of proteins and vaccines*, Marcel Dekker, New York, 1996.
71. J. Yang and J. L. Cleland. Factors affecting the *in vitro* release of recombinant human interferon-gamma (rhIFN-gamma) from PLGA microspheres. *J. Pharm. Sci.* **86**:908–914 (1997).
72. A. P. Nicholas, C. McInnis, K. B. Gupta, W. W. Snow, D. F. Love, D. W. Mason, T. M. Ferrell, J. K. Staas, and T. R. Tice. The fate of biodegradable microspheres injected into rat brain. *Neurosci. Lett.* **323**:85–88 (2002).
73. T. G. Park, W. Lu, and G. Crotts. Importance of *in vitro* experimental conditions on protein release kinetics, stability and polymer degradation in protein encapsulated poly (-lactic acid-co-glycolic acid) microspheres. *J. Control. Release* **33**:211–222 (1995).
74. S. C. Piscitelli, W. G. Reiss, W. D. Figg, and W. P. Petros. Pharmacokinetic studies with recombinant cytokines. Scientific issues and practical considerations. *Clin. Pharmacokinet.* **32**:368–381 (1997).
75. A. Sanchez, M. Tobio, L. Gonzalez, A. Fabra, and M. J. Alonso. Biodegradable micro- and nanoparticles as long-term delivery vehicles for interferon-alpha. *Eur. J. Pharm. Sci.* **18**:221–229 (2003).
76. L. Chen, R. N. Apte, and S. Cohen. Characterization of PLGA microspheres for the controlled delivery of IL-1[alpha] for tumor immunotherapy. *J. Control. Release* **43**:261–272 (1997).
77. R. Gref, Y. Minamitake, M. T. Peracchia, V. Trubetskoy, V. Torchilin, and R. Langer. Biodegradable long-circulating polymeric nanospheres. *Science* **263**:1600–1603 (1994).